CONTINUOUS LAMBERTIAN SHAPE FROM SHADING: A PRIMAL-DUAL ALGORITHM

Hamza Ennaji[1], Noureddine Igbida[1,*] and Van Thanh Nguyen[2]

Abstract. The continuous Lambertian shape from shading is studied using a PDE approach in terms of Hamilton–Jacobi equations. The latter will then be characterized by a maximization problem. In this paper we show the convergence of discretization and propose to use the well-known Chambolle–Pock primal-dual algorithm to solve numerically the shape from shading problem. The saddle-point structure of the problem makes the Chambolle–Pock algorithm suitable to approximate solutions of the discretized problems.

Mathematics Subject Classification. 49L25, 62H35, 65K10, 49Q22, 78A05.

Received October 19, 2020. Accepted January 28, 2022.

1. Introduction

Shape from Shading (SfS) consists in reconstructing the $3D$ shape of an object from its given $2D$ image brightness. The shape of a surface $u(x_1, x_2)$ is related to the image brightness $\mathrm{I}(x_1, x_2)$ by the Horn image irradiance equation [27]:

$$\mathcal{R}(\mathbf{n}(x_1, x_2)) = \mathrm{I}(x_1, x_2), \tag{1.1}$$

where $\mathrm{I}(x_1, x_2)$ is the brightness greylevel measured in the image at point (x_1, x_2); $\mathcal{R}(\mathbf{n}(x_1, x_2))$ is the reflectance map and $\mathbf{n}(x_1, x_2)$ is the unit normal at point $(x_1, x_2, u(x_1, x_2))$ given by

$$\mathbf{n}(x_1, x_2) = \frac{1}{\sqrt{1 + |\nabla u(x_1, x_2)|^2}} (-\partial_{x_1} u(x_1, x_2), -\partial_{x_2} u(x_1, x_2), 1).$$

In (1.1), the brightness function $\mathrm{I}(x_1, x_2)$ is known since it is measured at each pixel of the brightness image. The implicit unknown is the surface $u(x_1, x_2)$, which has to be reconstructed.

In the case where the $2D$ brightness image is obtained *via* a camera performing an orthographic projection of a Lambertian surface with constant albedo equal to 1, that is, the brightness map I is equal to the cosine of the angle between the normal vector $\mathbf{n}$ to the surface and the direction of the source of light, the maximal brightness is equal to 1 and the minimal one is 0 (see *e.g.* [35]). In that case, if we suppose that the surface is illuminated by

[1] Institut de recherche XLIM-DMI, UMR-CNRS 6172, Faculté des Sciences et Techniques, Université de Limoges, Limoges, France.
[2] Department of Mathematics and Statistics, Quy Nhon University, Binh Dinh, Vietnam.
*Corresponding author: noureddine.igbida@unilim.fr.

a simple distant light source of direction $\boldsymbol{\ell} = (w_1, w_2, w_3) \in \mathbb{R}^3$, one has $\mathcal{R}(\mathbf{n}(x_1, x_2)) = \mathbf{n}(x_1, x_2) \cdot (w_1, w_2, w_3)$ and, by (1.1),

$$\mathrm{I}\sqrt{1 + |\nabla u|^2} + (\nabla u, -1) \cdot \boldsymbol{\ell} = 0. \tag{1.2}$$

This equation falls into the scope of Hamilton–Jacobi (HJ) equations

$$H(\mathbf{x}, \nabla u) = 0 \ \text{ in } \Omega, \tag{1.3}$$

where the Hamiltonian H is defined by $H(\mathbf{x}, \mathbf{p}) = \mathrm{I}\sqrt{1 + |\mathbf{p}|^2} + (\mathbf{p}, -1) \cdot \boldsymbol{\ell}$, $\Omega \subset \mathbb{R}^2$ is the image domain and $\mathbf{x} = (x_1, x_2)$ is an image point. In particular, if the object is vertically enlightened, *i.e.* $\boldsymbol{\ell} = (0, 0, 1)$, one obtains the standard Eikonal equation

$$|\nabla u(x_1, x_2)| = \sqrt{\frac{1}{\mathrm{I}^2(x_1, x_2)} - 1}. \tag{1.4}$$

As pointed out in [17] (see also [44]), there are three major families of numerical methods allowing the resolution of the SfS problem. Namely, PDE methods (*cf.* [4, 9, 21, 22, 34, 39–41, 43]), optimization methods (*cf.* [15, 16, 29, 40]) and approximating the image irradiance equation (*cf.* [26, 36, 37]).

We are here interested in the study of the PDE formulation in terms of Hamilton–Jacobi equations (1.3). The theory of viscosity solutions [13, 14, 33] provides a suitable framework to study equations of the form (1.3). Applications of the viscosity theory to the SfS problem go back to the works of Lions *et al.* [34, 41] and the work of Prados *et al.* [39]. In addition, a lot of work was done to deal with more realistic and complicated models (see *e.g.* [2, 12, 42] and the references therein). Several difficulties arise while dealing with the SfS problem, namely compatibility of boundary conditions and the degeneracy of the Hamiltonian. It is well known that for (1.3) coupled with the boundary condition $u = g$ on $\partial\Omega$, to admit a solution one needs to check that $g(\mathbf{x}) - g(\mathbf{y}) \leq d_\sigma(\mathbf{y}, \mathbf{x})$ for all $\mathbf{x}, \mathbf{y} \in \partial\Omega$, where d_σ is the intrinsic distance associated to the Hamiltonian, which will be defined later. In addition, imposing only boundary conditions is not sufficient to ensure the uniqueness of solution to the Hamilton–Jacobi equations (1.3). It turns out that the set of degeneracy of the distance d_σ, called the Aubry set, plays the role of a uniqueness set for (1.3) (see *e.g.* [23]). In the case of Eikonal equation (1.4), the Aubry set $\mathcal{A}$ can be taken as the zero set $[k = 0]$ of $k = \sqrt{\mathrm{I}^{-2} - 1}$. In other words, it corresponds to the points with maximal intensity I, *i.e.* $\mathrm{I}(x_1, x_2) = 1$ so that the right hand side in (1.4) vanishes. Most of the authors (*cf.* [7, 39, 41] for example) choose to regularize the equation to avoid these points. We will not encounter this difficulty in our approach since we do not need to deal with the inverse of possibly vanishing functions. We only need to perform projections onto Euclidean balls whose radii may be equal to zero. Recall that the degeneracy of the Hamiltonian is intimately related to the so called concave/convex ambiguity [28, 43] where two different surfaces may have the same brightness I so that the reconstructed shape may be different from the original one. In the present paper, as in [7, 8], this can be tackled by looking for the maximal viscosity subsolution.

In this paper, following our approach in [19], we will characterize the maximal viscosity subsolution of (1.3) in terms of a concave maximization problem. We then associate it with a dual problem and exploit the saddle-point structure to approximate the solution of (1.3) using the Chambolle–Pock (CP) algorithm. Our approach lies between the PDE and optimization methods, since we start by characterizing the maximal viscosity subsolution of the HJ equation thanks to the intrinsic metric of the Hamiltonian and we end up with an optimization problem under gradient constraint. Moreover, the convergence of discretization is also studied in detail.

The paper is organized as follows. In Section 2, we start by recalling briefly some notions on HJ equations, and we present the maximization problem following [19] as well as related duality results in continuous setting. Section 3 is devoted to the discretization issue and the proof of convergence. We show how to apply the CP algorithm and present some numerical results to illustrate our approach in Section 4.

2. Maximization problem and duality in continuous setting

Notations

Throughout this paper, Ω is a bounded regular domain of $\mathbb{R}^N$ ($N = 2$ in Sect. 4). We denote by $\mathcal{D}(\Omega)$ the space of functions $u \in C^\infty(\Omega)$ with compact support in Ω, and $\mathcal{D}'(\Omega)$ the space of distributions in Ω. We use the standard notation for the Sobolev spaces

$$H^1(\Omega) = \left\{ u \in L^2(\Omega) : \ \nabla u \in L^2(\Omega) \right\},$$

and $H_0^1(\Omega) = \overline{\mathcal{D}(\Omega)}$, the closure of $\mathcal{D}(\Omega)$ in $H^1(\Omega)$. Recall that there exists a unique linear and continuous mapping $\gamma_0 : H^1(\Omega) \to L^2(\partial\Omega)$ such that $\gamma_0(u) = u_{|\partial\Omega}$ for all $u \in H^1(\Omega) \cap C(\overline{\Omega})$. We define $H^{1/2}(\partial\Omega) = \gamma_0(H^1(\Omega))$ and $H^{-1/2}(\partial\Omega)$ its dual. We recall the space

$$H_{\mathrm{div}}(\Omega) = \left\{ \boldsymbol{\phi} \in L^2(\Omega)^N : \ \mathrm{div}(\boldsymbol{\phi}) \in L^2(\Omega) \right\}.$$

There exists a continuous trace operator $\gamma_{\boldsymbol{\nu}} : H_{\mathrm{div}}(\Omega) \to H^{-1/2}(\partial\Omega)$ such that $\gamma_{\boldsymbol{\nu}}(\boldsymbol{\phi}) = \boldsymbol{\phi} \cdot \boldsymbol{\nu}$ for any $\boldsymbol{\phi} \in \mathcal{D}(\overline{\Omega})^N$, where $\boldsymbol{\nu}$ is outward unit field normal to $\partial\Omega$. This being said, we have thanks to Gauss's Theorem

$$\langle \gamma_0(u), \gamma_{\boldsymbol{\nu}}(\boldsymbol{\phi}) \rangle_{H^{1/2}, H^{-1/2}} = \int_\Omega \boldsymbol{\phi} \cdot \nabla u \, \mathrm{d}x + \int_\Omega u \, \mathrm{div}(\boldsymbol{\phi}) \mathrm{d}x \quad \text{for all} \ \ u \in H^1(\Omega), \boldsymbol{\phi} \in H_{\mathrm{div}}(\Omega).$$

Finally, we denote by $\mathcal{M}_b(\overline{\Omega})^N$ the space of $\mathbb{R}^N$-valued finite Radon measures on $\overline{\Omega}$.

For the rest of this section we recall the metric character of HJ equations, and introduce duality results, which will be useful to the proof of convergence of discretization in Section 3.

2.1. Metric character of HJ equations

Let $H : \overline{\Omega} \times \mathbb{R}^N \to \mathbb{R}$ be a continuous Hamiltonian satisfying the three following assumptions, for $\mathbf{x} \in \overline{\Omega}$, $Z(\mathbf{x}) := \{ \mathbf{p} \in \mathbb{R}^N : \ H(\mathbf{x}, \mathbf{p}) \leq 0 \}$,

(H1) coercivity: $Z(\mathbf{x})$ is compact;
(H2) convexity: $Z(\mathbf{x})$ is convex;
(H3) $H(\mathbf{x}, 0) \leq 0$, *i.e.* $0 \in Z(\mathbf{x})$.

We consider the following HJ equation

$$H(\mathbf{x}, \nabla u) = 0, \ \mathbf{x} \in \Omega. \tag{2.1}$$

A continuous function $u \colon \Omega \to \mathbb{R}$ is said to be a viscosity subsolution (respectively supersolution) of (2.1) if $H(\mathbf{x}, \nabla\phi(\mathbf{x})) \leq 0$ (respectively $H(\mathbf{x}, \nabla\phi(\mathbf{x})) \geq 0$) for any $\mathbf{x} \in \Omega$ and any C^1 function ϕ such that $u - \phi$ has a *strict* local maximizer (respectively minimizer) at $\mathbf{x}$. Finally, u is a viscosity solution of (2.1) if it is both a subsolution and a supersolution. We denote by $\mathcal{S}_H^-(\Omega)$ (respectively $\mathcal{S}_H^+(\Omega)$) the family of viscosity subsolutions (respectively supersolutions) of (2.1).

For $\mathbf{x} \in \overline{\Omega}$, we define the support function of the 0-sublevel set $Z(\mathbf{x})$ by

$$\sigma(\mathbf{x}, \mathbf{q}) := \sup \mathbf{q} \cdot Z(\mathbf{x}) = \sup\{\mathbf{q} \cdot \mathbf{p} \mid \ \mathbf{p} \in Z(\mathbf{x})\} \quad \text{for } \mathbf{q} \in \mathbb{R}^N. \tag{2.2}$$

The assumptions (H1)–(H3) ensure that σ is a possibly degenerate Finsler metric, *i.e.*, σ is a continuous nonnegative function in $\overline{\Omega} \times \mathbb{R}^N$, convex and positively homogeneous with respect to the second variable $\mathbf{q}$. Due to the assumption (H3), $\sigma(\mathbf{x}, \mathbf{q})$ can possibly be equal to 0 for $\mathbf{q} \neq 0$, which leads to the degeneracy and its dual σ^*, as defined below, may take the value $+\infty$. Here, the dual σ^* (also called polar) is defined by

$$\sigma^*(\mathbf{x}, \mathbf{p}) := \sup_{\mathbf{q}} \{\mathbf{p} \cdot \mathbf{q} \mid \ \sigma(\mathbf{x}, \mathbf{q}) \leq 1\}. \tag{2.3}$$

Let us define the intrinsic distance by

$$d_\sigma(\mathbf{x}, \mathbf{y}) := \inf_{\substack{\zeta \in \mathrm{Lip}([0,1];\overline{\Omega}) \\ \zeta(0)=\mathbf{x},\zeta(1)=\mathbf{y}}} \int_0^1 \sigma(\zeta(t), \dot{\zeta}(t)) \mathrm{d}t, \tag{2.4}$$

which is a quasi-distance, *i.e.* satisfying $d_\sigma(\mathbf{x}, \mathbf{x}) = 0$ and the triangular inequality, but not necessarily symmetric. We summarize some basic characterizations of subsolutions in terms of the intrinsic distance d_σ.

Proposition 2.1 ([19, 23, 30]).

(1) *Compatibility condition:* $v \in \mathcal{S}_H^-(\Omega)$ *if and only if* $v(\mathbf{x}) - v(\mathbf{y}) \le d_\sigma(\mathbf{y}, \mathbf{x})$ *for any* $\mathbf{x}, \mathbf{y} \in \Omega$.
(2) *We have*

$$u(\mathbf{x}) - u(\mathbf{y}) \le d_\sigma(\mathbf{y}, \mathbf{x}) \iff \sigma^*(\mathbf{x}, \nabla u) \le 1 \quad a.e. \text{ in } \Omega.$$

2.2. A maximization problem and duality

Given a closed subset $D \subset \overline{\Omega}$ (typically $D = \partial\Omega$ or $D = \{\mathbf{x}\}$ for some $\mathbf{x} \in \overline{\Omega}$), we consider the following HJ equation

$$\begin{cases} H(\mathbf{x}, \nabla u) = 0 & \text{in } \Omega \setminus D \\ u = g & \text{on } D \end{cases} \tag{2.5}$$

where $g: D \to \mathbb{R}$ is a continuous function satisfying the compatibility condition

$$g(\mathbf{x}) - g(\mathbf{y}) \le d_\sigma(\mathbf{y}, \mathbf{x}) \quad \text{for any } \mathbf{x}, \mathbf{y} \in D. \tag{2.6}$$

Thanks to Proposition 2.1, the following result allows us to approach the SfS problem *via* a maximization problem.

Theorem 2.2 ([19]). *The unique maximal viscosity subsolution of the problem* (2.5) *can be recovered via the following maximization problem*

$$(\mathrm{M}) := \max_{u \in W^{1,\infty}(\Omega)} \left\{ \int_\Omega u(\mathbf{x}) \mathrm{d}\mathbf{x}, \ \sigma^*(\mathbf{x}, \nabla u(\mathbf{x})) \le 1 \text{ and } u = g \text{ on } D \right\}. \tag{2.7}$$

This problem can be linked to the following dual problem. For simplicity, we will state it for the case $D = \partial\Omega$ (which is essentially the case for the numerical examples in Sect. 4.3).

Theorem 2.3. *Under the assumptions* (H1)–(H3) *we have*

$$\max_{u \in W^{1,\infty}(\Omega)} \left\{ \int_\Omega u(\mathbf{x}) \mathrm{d}\mathbf{x}, \ \sigma^*(\mathbf{x}, \nabla u(\mathbf{x})) \le 1 \text{ and } u = g \text{ on } \partial\Omega \right\}$$
$$= \inf_{\boldsymbol{\phi} \in L^2(\Omega)^N} \left\{ \int_\Omega \sigma(\mathbf{x}, \boldsymbol{\phi}(\mathbf{x})) \mathrm{d}\mathbf{x} - \langle g, \boldsymbol{\phi} \cdot \boldsymbol{\nu} \rangle_{H^{1/2}, H^{-1/2}} : -\mathrm{div}(\boldsymbol{\phi}) = 1 \text{ in } \mathcal{D}'(\Omega) \right\} := (\mathrm{OF}). \tag{2.8}$$

Proof. To prove the duality between (M) and (OF) in Theorem 2.3, we use a perturbation technique as follows. Define on $L^2(\Omega)^N$ the following functional

$$E(\mathbf{p}) := -\sup \left\{ \int_\Omega u(\mathbf{x}) \mathrm{d}\mathbf{x} : u \in \mathrm{Lip}(\Omega), \ \sigma^*(\mathbf{x}, \nabla u(\mathbf{x}) - \mathbf{p}(\mathbf{x})) \le 1, \ u = g \text{ on } \partial\Omega \right\}.$$

Then, one can check that E is convex and lower semicontinuous. To compute E^* we start by observing that since $u = g$ on $\partial\Omega$, we can assume thanks to trace lifting Theorem (see *e.g.* [6], Thm. III.2.22) that $g = \gamma_0(w)$ for some w in $H^1(\Omega)$, and $u = \xi + w$ with $\xi \in H_0^1(\Omega) \cap W^{1,\infty}(\Omega)$, where $\gamma_0 : H^1(\Omega) \to L^2(\partial\Omega)$ is the trace operator on $H^1(\Omega)$.

We then have for any $\boldsymbol{\phi} \in L^2(\Omega)^N$:

$$
E^*(\boldsymbol{\phi}) = \sup_{\mathbf{p} \in L^2(\Omega)^N} \int_\Omega \boldsymbol{\phi}(\mathbf{x}) \cdot \mathbf{p}(\mathbf{x})\, \mathrm{d}\mathbf{x} - E(\mathbf{p})
$$

$$
= \sup_{\mathbf{p} \in L^2(\Omega)^N, \xi \in H_0^1(\Omega)} \left\{ \int_\Omega \boldsymbol{\phi}(\mathbf{x}) \cdot \mathbf{p}(\mathbf{x})\, \mathrm{d}\mathbf{x} + \int_\Omega \xi(\mathbf{x})\mathrm{d}\mathbf{x} + \int_\Omega w(\mathbf{x})\mathrm{d}\mathbf{x} : \sigma^*(\mathbf{x}, \nabla(\xi + w) - \mathbf{p}) \le 1 \right\}.
$$

Set $\mathbf{q} = \nabla(\xi + w) - \mathbf{p}$ we get $\mathbf{p} = \nabla(\xi + w) - \mathbf{q}$, we then have

$$
E^*(\boldsymbol{\phi}) = \sup_{\mathbf{q} \in L^2(\Omega)^N, \xi \in H_0^1(\Omega)} \left\{ \int_\Omega \boldsymbol{\phi} \cdot (\nabla(\xi + w) - \mathbf{q})\mathrm{d}\mathbf{x} + \int_\Omega \xi \mathrm{d}\mathbf{x} + \int_\Omega w\, \mathrm{d}\mathbf{x} : \sigma^*(\mathbf{x}, \mathbf{q}(\mathbf{x})) \le 1 \right\}
$$

$$
= \sup_{\substack{\xi \in H_0^1(\Omega) \\ \mathbf{q} \in L^2(\Omega)^N, \ \sigma^*(\mathbf{x}, \mathbf{q}(\mathbf{x})) \le 1}} \left\{ \int_\Omega \boldsymbol{\phi} \cdot \nabla \xi \mathrm{d}\mathbf{x} + \int_\Omega \xi \mathrm{d}\mathbf{x} + \int_\Omega \boldsymbol{\phi} \cdot \nabla w \mathrm{d}\mathbf{x} + \int_\Omega w \mathrm{d}\mathbf{x} - \int_\Omega \boldsymbol{\phi} \cdot \mathbf{q}\mathrm{d}\mathbf{x} \right\}.
$$

The last quantity is finite if we impose that $\int_\Omega \boldsymbol{\phi} \cdot \nabla \xi \mathrm{d}\mathbf{x} + \int_\Omega \xi \mathrm{d}\mathbf{x} = 0$ for all $\xi \in H_0^1(\Omega)$, which means that $-\mathrm{div}(-\boldsymbol{\phi}) = 1$ and consequently $\boldsymbol{\phi} \in H_{\mathrm{div}}(\Omega)$. Thus the normal trace of $\boldsymbol{\phi}$ is well-defined and $\boldsymbol{\phi} \cdot \boldsymbol{\nu} \in H^{-1/2}(\partial\Omega)$. Taking $\mu = -\boldsymbol{\phi} \cdot \boldsymbol{\nu}$, then $-\mathrm{div}(-\boldsymbol{\phi}) = 1 - \mu$ in $\mathcal{D}'(\mathbb{R}^N)$ and therefore, for such a $\boldsymbol{\phi}$, integrating by parts we get

$$
E^*(-\boldsymbol{\phi}) = \sup_{\mathbf{q} \in L^2(\Omega)^N} \left\{ \int_\Omega \boldsymbol{\phi} \cdot \mathbf{q}\, \mathrm{d}\mathbf{x} : \sigma^*(\mathbf{x}, \mathbf{q}(\mathbf{x})) \le 1 \right\} + \langle w, \mu \rangle_{H^{1/2}, H^{-1/2}}
$$

$$
= \int_\Omega \sigma(\mathbf{x}, \boldsymbol{\phi})\mathrm{d}\mathbf{x} - \langle g, \boldsymbol{\phi} \cdot \boldsymbol{\nu} \rangle_{H^{1/2}, H^{-1/2}}.
$$

(2.9)

Finally,

$$
\max(\mathrm{M}) = -E(0) = -E^{**}(0) = -\sup_{\boldsymbol{\phi} \in L^2(\Omega)^N} -E^*(-\boldsymbol{\phi}) = \inf_{\boldsymbol{\phi} \in L^2(\Omega)^N} E^*(-\boldsymbol{\phi}) = \inf(\mathrm{OF}),
$$

as desired. $\qquad\square$

Remark 2.4. Notice here that the proof remains to be true also for the general maximization problem

$$
\max_{u \in W^{1,\infty}(\Omega)} \left\{ \int_\Omega u(\mathbf{x})\, \rho(\mathbf{x})\mathrm{d}\mathbf{x}, \ \sigma^*(\mathbf{x}, \nabla u(\mathbf{x})) \le 1 \text{ and } u = g \text{ on } \partial\Omega \right\},
$$

where $\rho \in L^2(\Omega)$. See that dealing with this duality, the trace of the dual variable $\boldsymbol{\phi}$ on the boundary plays an important role in the dual problem. For the context of general Radon measure ρ, one can see the paper [19]. In this case one needs to deal with technical functional space $\mathcal{DM}^p(\Omega)$ (space of vector fields $\boldsymbol{\phi} \in L^p(\Omega)^N$ whose divergence are bounded measures). On such a space, one can give a sense to $\boldsymbol{\phi} \cdot \boldsymbol{\nu}$, the normal trace of $\boldsymbol{\phi}$ on $\partial\Omega$ (cf. [19]). For a different duality approach with free Radon measure boundary trace one can see the paper [20].

Remark 2.5. The so-called Aubry set, denoted by $\mathcal{A}$, is defined as the set where the quasi-distance d_σ degenerates, i.e. it fails to be equivalent to the Euclidean one. More precisely, the Aubry set consists of points $x \in \Omega$ such that there exists cycles $(\zeta_n)_n \in \mathrm{Lip}([0,1]; \overline{\Omega})$ with $\zeta_n(0) = \mathbf{x}$ and $\zeta_n(1) = \mathbf{y}$, with positive Euclidean length, i.e. $l(\zeta_n) > \delta > 0$ for some $\delta > 0$ and

$$
\inf_n \left\{ \int_0^1 \sigma(\zeta_n(t), \dot{\zeta}_n(t))\mathrm{d}t \right\} = 0.
$$

Prescribing a boundary value on $\partial\Omega$ does not guarantee the uniqueness of viscosity solutions to (2.1) unless if $\mathcal{A} = \emptyset$. The Aubry set $\mathcal{A}$ appears then to be a uniqueness set for (2.1) (see [23] for details).
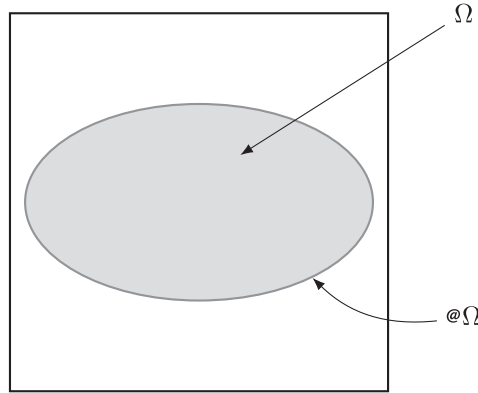
FIGURE 1. An object and its occluding boundary.

As a typical example, for the case of the vertical light $\boldsymbol{\ell} = (0, 0, 1)$ and $u = 0$ on $\partial\Omega$, the orthographic SfS problem amounts to solve the following Eikonal equation

$$\begin{cases} |\nabla u| = k & \text{in} \quad \Omega \\ \quad u = 0 & \text{on} \quad \partial\Omega \end{cases} \tag{2.10}$$

where $k(\mathbf{x}) = \sqrt{\mathrm{I}^{-2}(\mathbf{x}) - 1}$. In this case, the duality in Theorem 2.3 reads as

$$\max_{u \in W^{1,\infty}(\Omega)} \left\{ \int_\Omega u \mathrm{d}\mathbf{x} : |\nabla u| \le k, \ u = 0 \text{ on } \partial\Omega \right\} = \inf_{\boldsymbol{\phi} \in L^2(\Omega)^N} \left\{ \int_\Omega k(\mathbf{x})|\boldsymbol{\phi}|\mathrm{d}\mathbf{x} : -\mathrm{div}(\boldsymbol{\phi}) = 1 \text{ in } \mathcal{D}'(\Omega) \right\}. \tag{2.11}$$

The Aubry set $\mathcal{A}$ can then be taken as the zero set $[k = 0]$ of $k = \sqrt{\mathrm{I}^{-2} - 1}$, which corresponds to the points with maximal intensity I, *i.e.* $\mathrm{I}(\mathbf{x}) = 1$ so that $k(\mathbf{x})$ vanishes. As we will see in the next section, dealing with nonempty Aubry set does not represent an obstacle in our approach. Contrary to the works (*e.g.* [7, 39, 41]) where the authors approximate the degenerate HJ equation *via* non-degenerate one (typically, by considering (2.10) with $k_\epsilon = \max(k, \epsilon)$ for $\epsilon > 0$), the only step where we deal with degeneracy points is the projection onto a ball of radius k, which may be equal to zero.

Remark 2.6 (Boundary conditions)**.** It is well known that a natural choice for boundary conditions is the Dirichlet boundary condition. As pointed out in [17], the images we will consider in this paper contain an occluding boundary (see Fig. 1) which will be taken as the boundary $\partial\Omega$. Particularly, assuming that the object is placed on a flat table suggests taking $u = 0$ on $\partial\Omega$ or more generally, if the height g of the surface on which is placed is known one can take $u = g$ on $\partial\Omega$.

3. DISCRETIZATION

In this section we focus on the the discretized (finite-dimensional) problems associated with the problems (M) and (OF).

3.1. Discretization of the domain and operators

Let $\Omega \subset \mathbb{R}^N$ with $N = 2$ in the case of an image, which can be taken as $\Omega = [0, 1]^2$. Following [10], we discretize the domain Ω using a regular grid $m \times n$: $\{(ih, jh) : \ 1 \le i \le m, 1 \le j \le n\}$ for a fixed $h > 0$. We

denote by $D_d = \{(i,j) : (ih, jh) \in D\}$ the indexes whose spatial positions belong to D and by $u_{i,j}$ the values of u at (ih, jh). The space $X = \mathbb{R}^{m \times n}$ is equipped with a scalar product and an associated norm as follows:

$$\langle u, v \rangle = h^2 \sum_{i=1}^{m} \sum_{j=1}^{n} u_{i,j} v_{i,j} \quad \text{and} \quad \|u\| = \sqrt{\langle u, u \rangle}.$$

For $1 \le i \le m$ and $1 \le j \le n$, we define the components of the discrete gradient operator *via* finite differences:

$$(\nabla_h u)^1_{i,j} = \begin{cases} \frac{u_{i+1,j} - u_{i,j}}{h} & \text{if } i < m, \\ 0 & \text{if } i = m, \end{cases} \qquad (\nabla_h u)^2_{i,j} = \begin{cases} \frac{u_{i,j+1} - u_{i,j}}{h} & \text{if } j < n, \\ 0 & \text{if } j = n. \end{cases} \tag{3.1}$$

Then the discrete gradient $\nabla_h : X \longrightarrow Y = \mathbb{R}^{m \times n \times 2}$ given by $(\nabla_h u)_{i,j} = \left((\nabla_h u)^1_{i,j}, (\nabla_h u)^2_{i,j} \right)$. Similar to the continuous setting, we define a discrete divergence operator $\text{div}_h : Y \to X$, which is the minus of the adjoint of ∇_h, given by $\text{div}_h = -\nabla_h^*$. That is, $\langle -\text{div}_h \phi, u \rangle_X = \langle \phi, \nabla_h u \rangle_Y$ for any $\phi = (\phi^1, \phi^2) \in Y$ and $u \in X$. It follows that div is explicitly given by (see *e.g.* [10])

$$(\text{div}_h \phi)_{i,j} = \begin{cases} \frac{\phi^1_{i,j}}{h} & \text{if } i = 1 \\ \frac{\phi^1_{i,j} - \phi^1_{i-1,j}}{h} & \text{if } 1 < i < m \\ \frac{-\phi^1_{m-1,j}}{h} & \text{if } i = m \end{cases} + \begin{cases} \frac{\phi^2_{i,j}}{h} & \text{if } j = 1 \\ \frac{\phi^2_{i,j} - \phi^2_{i,j-1}}{h} & \text{if } 1 < j < n \\ \frac{-\phi^2_{i,n-1}}{h} & \text{if } j = n. \end{cases} \tag{3.2}$$

Proposition 3.1 ([10,11])**.** *Under the above-mentioned definitions and notations, one has that*

– *The adjoint operator of ∇_h is $\nabla_h^* = -\text{div}_h$.*
– *Its norm satisfies: $\|\nabla_h\|^2 = \|\text{div}_h\|^2 \le 8/h^2$.*

3.2. Discretization of the optimization problem

Based on the discrete gradient and divergence operators, we propose a discrete version of (M) as follows

$$(\text{M})_d : \min_{\substack{u \in X \\ u_{i,j} = g_{i,j} \ \forall (i,j) \in D_d}} \left\{ -h^2 \sum_{i=1}^{m} \sum_{j=1}^{n} u_{i,j} + \mathbb{I}_{B_{\sigma^*}} (\nabla_h u) \right\} \tag{3.3}$$

where $B_{\sigma^*} := \{v \in Y : \sigma^*(ih, jh, v_{i,j}) \le 1, \ \forall (i,j)\}$ the unit ball w.r.t. σ^*, and $\mathbb{I}_{B_{\sigma^*}}$ is the indicator function in the sense of convex analysis, that is,

$$\mathbb{I}_{B_{\sigma^*}}(v) = \begin{cases} 0 & \text{if } v \in B_{\sigma^*} \\ +\infty & \text{otherwise.} \end{cases}$$

In other words, the discrete version $(\text{M})_d$ can be written as

$$\min_{u \in X} \mathcal{F}_h(u) + \mathcal{G}_h(\nabla_h u), \tag{3.4}$$

where

$$\mathcal{F}_h(u) = \begin{cases} -h^2 \sum_{i=1}^{m} \sum_{j=1}^{n} u_{i,j} & \text{if } u_{i,j} = g_{i,j} \ \forall (i,j) \in D_d \\ +\infty & \text{otherwise} \end{cases}, \text{ and } \mathcal{G}_h = \mathbb{I}_{B_{\sigma^*}}. \tag{3.5}$$

Let $u^* \in X^*$, we then have

$$\mathcal{F}_h^*(u^*) = \sup_{u \in X} \langle u, u^* \rangle_X - \mathcal{F}_h(u) = \sup_{\substack{u \in X \\ u_{i,j}=g_{i,j} \ \forall (i,j) \in D_d}} h^2 \sum_{i=1}^m \sum_{j=1}^n u_{i,j} u_{i,j}^* + h^2 \sum_{i=1}^m \sum_{j=1}^n u_{i,j}$$

$$= \sup_{\substack{u \in X \\ u_{i,j}=g_{i,j} \ \forall (i,j) \in D_d}} h^2 \sum_{i=1}^m \sum_{j=1}^n u_{i,j}(u_{i,j}^* + 1) \tag{3.6}$$

$$= \begin{cases} h^2 \sum_{(i,j) \in D_d} g_{i,j}\left(u_{i,j}^* + 1\right) & \text{if } -u_{i,j}^* = 1 \text{ for } (i,j) \notin D_d \\ +\infty & \text{otherwise.} \end{cases}$$

It follows that

$$\mathcal{F}_h^*(\mathrm{div}_h \boldsymbol{\phi}) = \begin{cases} h^2 \sum_{(i,j) \in D_d} g_{i,j}((\mathrm{div}_h \boldsymbol{\phi})_{i,j} + 1) & \text{if } (-\mathrm{div}_h \boldsymbol{\phi})_{i,j} = 1 \text{ for } (i,j) \notin D_d \\ +\infty & \text{otherwise.} \end{cases}$$

On the other hand, we have for $\mathbf{q} = (q^1, q^2) \in Y^*$

$$\mathcal{G}_h^*(\mathbf{q}) = \sup_{\mathbf{p}=(p^1,p^2) \in Y} \langle \mathbf{p}, \mathbf{q} \rangle_Y - \mathcal{G}_h(\mathbf{p}) = \sup_{\mathbf{p} \in B_{\sigma^*}} h^2 \sum_{i=1}^m \sum_{j=1}^n \left(p_{i,j}^1 q_{i,j}^1 + p_{i,j}^2 q_{i,j}^2\right) = h^2 \sum_{i=1}^m \sum_{j=1}^n \sigma\left(ih, jh, \mathbf{q}_{i,j}\right). \tag{3.7}$$

Consequently, the corresponding discrete dual problem is given by

$$(\mathrm{OF})_d : \max_{\boldsymbol{\phi} \in Y} \{ -\mathcal{F}_h^*(\mathrm{div}_h \boldsymbol{\phi}) - \mathcal{G}_h^*(\boldsymbol{\phi}) \}$$

$$= - \min_{\substack{\boldsymbol{\phi} \in Y \\ (-\mathrm{div}_h \boldsymbol{\phi})_{i,j}=1 \text{ for } (i,j) \notin D_d}} h^2 \left\{ \sum_{i=1}^m \sum_{j=1}^n \sigma(ih, jh, \boldsymbol{\phi}_{i,j}) + \sum_{(i,j) \in D_d} g_{i,j}((\mathrm{div}_h \boldsymbol{\phi})_{i,j} + 1) \right\}. \tag{3.8}$$

In particular, for the case of Eikonal equations $|\nabla u(\mathbf{x})| = k(\mathbf{x})$, the primal-dual relations can be explicitly written as

$$\min_{\substack{u \in X \\ u_{i,j}=g_{i,j} \ \forall (i,j) \in D_d}} \left\{ -h^2 \sum_{i=1}^m \sum_{j=1}^n u_{i,j} + \mathbb{I}_{B(0,k_{i,j})}(\nabla_h u_{i,j}) \right\}$$

$$= - \min_{\substack{\boldsymbol{\phi} \in Y \\ (-\mathrm{div}_h \boldsymbol{\phi})_{i,j}=1 \text{ for } (i,j) \notin D_d}} h^2 \left\{ \sum_{i=1}^m \sum_{j=1}^n k_{i,j} \|\boldsymbol{\phi}_{i,j}\| + \sum_{(i,j) \in D_d} g_{i,j}((\mathrm{div}_h \boldsymbol{\phi})_{i,j} + 1) \right\}, \tag{3.9}$$

where $\mathbb{I}_{B(0,k_{i,j})}$ is the indicator function of the Euclidean ball with center 0 and radius $k_{i,j}$, the latter being the value of k at (ih, jh).

To end this subsection, let us recall that a pair $(u, \boldsymbol{\phi}) \in X \times Y$ solves the primal and dual problems $(\mathrm{M})_d$ and $(\mathrm{OF})_d$ if and only if

$$\mathrm{div}_h(\boldsymbol{\phi}) \in \partial \mathcal{F}_h(u) \text{ and } \boldsymbol{\phi} \in \partial \mathcal{G}_h(\nabla_h u), \tag{3.10}$$

or equivalently, they satisfy the following system

$$\begin{cases} -(\mathrm{div}(\boldsymbol{\phi}))_{i,j} = 1 & \text{for } (i,j) \notin D_d \\ \boldsymbol{\phi}_{i,j} \cdot \nabla_h u_{i,j} = \sigma\left(ih, jh, \boldsymbol{\phi}_{i,j}\right) & \text{for all } (i,j) \\ u_{i,j} = g_{i,j} & \text{for every } (i,j) \in D_d. \end{cases} \tag{3.11}$$
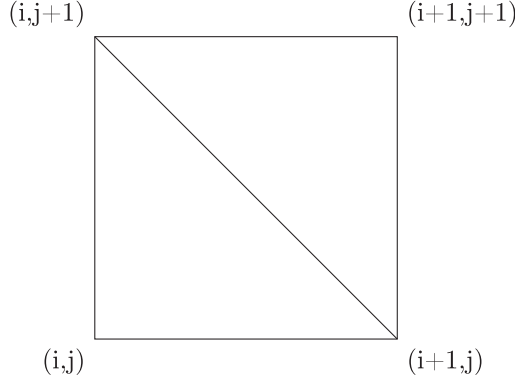
FIGURE 2. Sub-triangles.

3.3. The convergence of discretization

In this subsection, we will show a result on the convergence of discretization, *i.e.* where the solutions of the discrete optimization and its discrete dual problem converge to the ones of the corresponding problems in continuous setting. For technical reason (see Rems. 3.4, 3.5) we focus on the non-degenerate case; *i.e.* $H(\mathbf{x}, 0) < 0$ for any $\mathbf{x} \in \Omega$, as well as to the case where $g \equiv 0$.

First, let us describe how to interpolate elements of X and Y. We know the values of $u_h \in X$ at the vertices $(i, j), (i, j + 1), (i + 1, j + 1), (i + 1, j)$ of a small square (see Fig. 2). We interpolate $u_h \in X$ by piecewise affine functions on the sub-triangles, *i.e.* taking $\tilde{u}_h \in L^2(\Omega)$ as an affine function on the sub-triangles and coincides with u_h on all the vertices. Then $\tilde{u}_h$ is a Lipschitz function and its gradient is, by the definition of $\tilde{u}_h$, given by

$$\nabla \tilde{u}_h(x, y) = \left(\frac{u_h(i + 1, j) - u_h(i, j)}{h}, \frac{u_h(i, j + 1) - u_h(i, j)}{h} \right) \tag{3.12}$$

on the sub-triangle of the vertices $(i, j), (i, j + 1), (i + 1, j)$; and

$$\nabla \tilde{u}_h(x, y) = \left(\frac{u_h(i + 1, j + 1) - u_h(i, j + 1)}{h}, \frac{u_h(i + 1, j + 1) - u_h(i + 1, j)}{h} \right) \tag{3.13}$$

on the sub-triangle of the vertices $(i, j + 1), (i + 1, j + 1), (i + 1, j)$.

Let $\tilde{\boldsymbol{\phi}}_h \in L^2(\Omega)^2$ be an interpolation of $\boldsymbol{\phi}_h \in Y$ such that $\int_\Omega \sigma(x, \tilde{\boldsymbol{\phi}}_h) \mathrm{d}x = h^2 \sum_{i=1}^m \sum_{j=1}^n \sigma(ih, jh, (\boldsymbol{\phi}_h)_{i,j})$.

Proposition 3.2 (Convergence of discretization)**.** *Assume that the Finsler metric σ associated with the Hamiltonian H is non-degenerate (i.e. $H(\boldsymbol{x}, 0) < 0, \forall \boldsymbol{x} \in \overline{\Omega}$) and that $g = 0$. Let $u_h \in X$ and $\boldsymbol{\phi}_h = (\phi_h^1, \phi_h^2) \in Y$ be a pair of primal-dual solutions to the discrete optimization problem* $(\mathrm{M})_d$ *and its dual problem* (3.8). *Then $\tilde{u}_h \rightrightarrows u$ and $\tilde{\boldsymbol{\phi}}_h \rightharpoonup \boldsymbol{\phi}$ weakly* in $\mathcal{M}_b(\overline{\Omega})^N$, as the step size $h \to 0$. Moreover, u and $\boldsymbol{\phi}$ are optimal solutions to* (M) *and its dual problem, respectively, in the following sense*

$$(\mathrm{OF}) = \min_{\boldsymbol{\psi} \in \mathcal{M}_b(\overline{\Omega})^N} \left\{ \int_\Omega \sigma\left(\boldsymbol{x}, \frac{\boldsymbol{\psi}}{|\boldsymbol{\psi}|}(\boldsymbol{x}) \right) \mathrm{d}|\boldsymbol{\psi}|(\boldsymbol{x}) \ : \ -\mathrm{div}(\boldsymbol{\psi}) = 1 \ \ \text{in} \ \ \mathcal{D}'(\Omega) \right\}$$

$$= \int_\Omega \sigma\left(\boldsymbol{x}, \frac{\boldsymbol{\phi}}{|\boldsymbol{\phi}|}(\boldsymbol{x}) \right) \mathrm{d}|\boldsymbol{\phi}|(\boldsymbol{x}) = \int_\Omega u(\boldsymbol{x}) \mathrm{d}\boldsymbol{x}$$

$$= (\mathrm{M}), \tag{3.14}$$

where $\frac{\boldsymbol{\phi}}{|\boldsymbol{\phi}|}(\boldsymbol{x})$ is the density of $\boldsymbol{\phi}$ with respect to $|\boldsymbol{\phi}|$, the total variation of $\boldsymbol{\phi}$.

Proof. Since u_h is feasible for the discrete optimization problem $(M)_d$, its discrete gradient $\nabla_h u_h \in B_{\sigma^*}$ is bounded for all small $h > 0$. In other words, the sequences $\left\{ \frac{u_h(i+1,j) - u_h(i,j)}{h} \right\}$ and $\left\{ \frac{u_h(i,j+1) - u_h(i,j)}{h} \right\}$ are bounded for $h > 0$ and $i = 1, ..., m, j = 1, ..., n$. Following (3.12) and (3.13), the sequence $\{\tilde{u}_h\}$ is equi-Lipschitz. Combining with the fact that $u_h = 0$ on D_d, by Ascoli–Arzela's Theorem, up to a subsequence, $\tilde{u}_h$ converges uniformly to some Lipschitz function u on $\overline{\Omega}$ as the step size $h \to 0$. By the optimality of u_h and $\boldsymbol{\phi}_h$, we have

$$\mathcal{F}_h(u_h) + \mathcal{G}_h(\nabla_h u_h) = -\mathcal{F}_h^*(\mathrm{div}_h \boldsymbol{\phi}_h) - \mathcal{G}_h^*(\boldsymbol{\phi}_h).$$

More concretely,

$$h^2 \sum_{i=1}^{m} \sum_{j=1}^{n} u_{i,j} = h^2 \sum_{i=1}^{m} \sum_{j=1}^{n} \sigma(ih, jh, (\boldsymbol{\phi}_h)_{i,j})$$

or equivalently

$$\int_\Omega \tilde{u}_h \mathrm{d}\mathbf{x} = \int_\Omega \sigma\left(\mathbf{x}, \tilde{\boldsymbol{\phi}}_h\right) \mathrm{d}\mathbf{x}.$$

Since σ is non-degenerate and $\tilde{u}_h$ is bounded, $\tilde{\boldsymbol{\phi}}_h$ is also bounded in $L^1(\Omega)$. Hence, $\tilde{\boldsymbol{\phi}}_h \rightharpoonup \boldsymbol{\phi}$ weakly* in $\mathcal{M}_b(\overline{\Omega})^N$. Using the lower-semicontinuity of the integrand (see [3], Thm. 2.38), we deduce that

$$\int_\Omega \sigma\left(\mathbf{x}, \frac{\boldsymbol{\phi}}{|\boldsymbol{\phi}|}(\mathbf{x})\right) \mathrm{d}|\boldsymbol{\phi}|(\mathbf{x}) \le \lim_{h \to 0} \int_\Omega \sigma\left(\mathbf{x}, \tilde{\boldsymbol{\phi}}_h\right) \mathrm{d}\mathbf{x} = \lim_{h \to 0} \int_\Omega \tilde{u}_h \mathrm{d}\mathbf{x} = \int_\Omega u \mathrm{d}\mathbf{x}. \tag{3.15}$$

This implies that

$$(\mathrm{OF}) = \min_{\boldsymbol{\psi} \in \mathcal{M}_b(\overline{\Omega})^N} \left\{ \int_\Omega \sigma\left(\mathbf{x}, \frac{\boldsymbol{\psi}}{|\boldsymbol{\psi}|}\right) \mathrm{d}|\boldsymbol{\psi}| \; : \; -\mathrm{div}(\boldsymbol{\psi}) = 1 \; \text{ in } \; \mathcal{D}'(\Omega) \right\}$$

$$\le \int_\Omega \sigma\left(\mathbf{x}, \frac{\boldsymbol{\phi}}{|\boldsymbol{\phi}|}(\mathbf{x})\right) \mathrm{d}|\boldsymbol{\phi}|(\mathbf{x}) \le \int_\Omega u \mathrm{d}\mathbf{x} \le (\mathrm{M}).$$

By the duality result in the continuous setting given in Section 2 (Thm. 2.3), we deduce the optimality of u and $\boldsymbol{\phi}$. $\square$

Remark 3.3. In general we do not know if (OF) has a solution in $L^2(\Omega)^N$, even if we do believe that this is not true in general. We are convinced that the weak* convergence of $\tilde{\boldsymbol{\phi}}_h$ in $\mathcal{M}_b(\overline{\Omega})^N$, as the step size $h \to 0$, is optimal. For the special case where σ is given by the Euclidean norm, (OF) admits a solution in $L^2(\Omega)^N$ (see *e.g.* [18]).

Remark 3.4. See that in the case where σ is a degenerate Finsler metric, even if the duality between (OF) and (M) holds to be true and the dual problem (OF) still have a solution in $\mathcal{M}_b(\overline{\Omega})^N$, we loose the compactness of $\tilde{\boldsymbol{\phi}}_h$. However, we still have the uniform convergence of $\tilde{u}_h$ to the optimal solution of the maximization problem (M).

Remark 3.5. The convergence of $\tilde{\boldsymbol{\phi}}_h$, even in the non degenerate Finsler metric case, is more subtle. This is connected to the weak* convergence of $\tilde{\boldsymbol{\phi}}_h$ in $\mathcal{M}_b(\overline{\Omega})^N$, and the normal trace of Radon measure vectors valued measure whose divergence is a bounded measures. In other words, it is not clear how to handle the convergence of the boundary term $\sum_{(i,j) \in D_d} g_{i,j}((\mathrm{div}_h \boldsymbol{\phi})_{i,j} + 1)$ to the corresponding continuous one of the type $\langle g, \boldsymbol{\phi} \cdot \boldsymbol{\nu} \rangle$.

4. NUMERICAL RESOLUTION

In this section we focus on the case where the light direction is vertical, *i.e.* $\boldsymbol{\ell} = (0, 0, 1)$.

4.1. Saddle-point structure

As we pointed out in Section 3, the discrete version $(\mathrm{M})_d$ of (M) given by (3.4) can be rewritten in an inf-sup form as

$$\inf_{u \in X} \sup_{\phi \in Y} \mathcal{F}_h(u) + \langle \phi, \nabla_h u \rangle - \mathcal{G}_h^*(\phi) \tag{4.1}$$

where $\mathcal{F}_h$ and $\mathcal{G}_h$ are defined in (3.5). Both the functions $\mathcal{F}_h$ and $\mathcal{G}_h$ are lower-semicontinuous, convex and they are "proximable", *i.e.* we can compute their proximal operators:

$$\begin{aligned}
\mathbf{Prox}_{\tau \mathcal{F}_h}(u) &= \operatorname*{argmin}_{v \in X} \frac{1}{2} \|u - v\|^2 + \tau \mathcal{F}_h(v) \\
\mathbf{Prox}_{\eta \mathcal{G}_h}(\psi) &= \operatorname*{argmin}_{\phi \in Y} \frac{1}{2} \|\psi - \phi\|^2 + \eta \mathcal{G}_h(\phi)
\end{aligned} \tag{4.2}$$

where $\tau, \eta > 0$. Then the Chambolle–Pock algorithm [11] can be applied to (3.4).

Algorithm 1. Chambolle–Pock iterations.

1st step. Initialization: choose $\eta, \tau > 0$, $\theta \in [0,1]$, u^0 and take $\phi^0 = \nabla_h u^0$, $\bar{u}^0 = u^0$.
2nd step. For $k \leq \mathrm{Iter}_{max}$ do

$$\phi^{k+1} = \mathbf{Prox}_{\eta \mathcal{G}_h^*}\Big(\phi^k + \eta \nabla_h \big(\bar{u}^k\big)\Big);$$

$$u^{k+1} = \mathbf{Prox}_{\tau \mathcal{F}_h}\Big(u^k - \tau \nabla_h^*\big(\phi^{k+1}\big)\Big);$$

$$\bar{u}^{k+1} = u^{k+1} + \theta\Big(u^{k+1} - u^k\Big).$$

It was shown in [11] that when $\theta = 1$ and $\eta \tau \|\nabla_h\|^2 < 1$, the sequence $\{u^k\}$ converges to an optimal solution of (3.4). Contrary to the augmented Lagrangian approach in [19] (see also [5, 30, 31]), the Chambolle–Pock algorithm does not require to solve a Laplace equation at each iteration, we only need to perform some algebraic operations, namely the multiplication by apply the gradient and the divergence in each iteration. The Chambolle–Pock algorithm is easy to implement on Matlab which allows working on images easily contrary to the augmented Lagrangian approach which was implemented using FreeFem++ to solve linear PDEs.

In order to compute $\mathbf{Prox}_{\eta \mathcal{G}_h^*}$ we make use of the celebrated Moreau identity

$$\phi = \mathbf{Prox}_{\eta \mathcal{G}_h^*}(\phi) + \eta \mathbf{Prox}_{\eta^{-1} \mathcal{G}_h}(\phi/\eta), \ \forall \phi \in Y. \tag{4.3}$$

Moreover, $\mathbf{Prox}_{\eta^{-1} \mathcal{G}_h}$ is nothing but the projection onto $B(0, k_{i,j})$. Indeed

$$\begin{aligned}
\mathbf{Prox}_{\eta^{-1} \mathcal{G}_h}(\psi) &= \arg\min_{\mathbf{q} \in Y} \frac{1}{2} |\mathbf{q} - \psi|^2 + \frac{1}{\eta} \mathcal{G}_h(\mathbf{q}) \\
&= \arg\min_{q_{i,j} \in B(0, k_{i,j})} \frac{1}{2} |\mathbf{q} - \psi|^2 \\
&= \mathbf{Proj}_{B(0, k_{i,j})}(\psi_{i,j}).
\end{aligned} \tag{4.4}$$

Consequently,

$$\big(\mathbf{Prox}_{\eta \mathcal{G}_h^*}(\psi)\big)_{i,j} = \psi_{i,j} - \eta \mathbf{Proj}_{B(0, k_{i,j})}(\psi_{i,j}/\eta).$$

Let us now compute the proximal operator of $\mathcal{F}_h$. We have

$$\mathbf{Prox}_{\tau \mathcal{F}_h}(u) = \operatorname*{argmin}_{v \in X} \frac{1}{2} \|v - u\|^2 + \tau \mathcal{F}_h(v) = \operatorname*{argmin}_{v = g \text{ on } D_d} \frac{1}{2} \|v - u\|^2 - \tau h^2 \sum_{i=1}^{m} \sum_{j=1}^{n} v_{i,j}. \tag{4.5}$$

Writing the first-order optimality condition we get

$$(\mathbf{Prox}_{\tau\mathcal{F}_h}(u))_{i,j} - u_{i,j} - \tau = 0 \Leftrightarrow (\mathbf{Prox}_{\tau\mathcal{F}_h}(u))_{i,j} = u_{i,j} + \tau, \ \forall i = 1, ..., m, \ j = 1, ..., n. \tag{4.6}$$

So in practice, we update u_{n+1} *via* the previous formula and we then set its values to g on the Dirichlet domain.

If the input image u is of width m and height n, we suppose that the reconstruction domain is $\Omega = \{1, \cdots, m\} \times \{1, \cdots, n\}$. Since proximal parameters η and τ are to be chose such that $\eta\tau < \frac{8}{h^2}$, taking $h = 1$ allows fixing these parameters easily.

The details of the 2nd step in Algorithm 1 are then given by

– compute ϕ^{k+1}:

$$\begin{aligned} \bar{\phi}^{k+1} &= \phi^k + \eta\nabla_h\bar{u}^k \\ \phi_{i,j}^{k+1} &= \bar{\phi}_{i,j}^{k+1} - \eta\mathbf{Proj}_{B(0,k_{i,j})}\left(\bar{\phi}_{i,j}^{k+1}/\eta\right), \ 1 \le i \le m, 1 \le j \le n; \end{aligned} \tag{4.7}$$

– compute u^{k+1}:

$$\begin{aligned} v^{k+1} &= u^k + \tau\mathrm{div}_h\left(\phi^{k+1}\right) \\ u_{i,j}^{k+1} &= v_{i,j}^{k+1} + \tau, \ 1 \le i \le m, 1 \le j \le n. \end{aligned} \tag{4.8}$$

Remark 4.1. Another way to formulate the problem (M) (in the continuous setting) is to take

$$\mathcal{F}(u) = -\int_\Omega u\mathrm{d}\mathbf{x}, \ \text{and} \ \mathcal{G}(\mathbf{q}, v) = \begin{cases} 0 & \text{if } |\mathbf{q}| \le k \text{ and } v = g \text{ on } \partial\Omega \\ \infty & \text{otherwise}, \end{cases}$$

for all $u \in W^{1,\infty}(\Omega)$, and $(\mathbf{q}, v) \in L^\infty(\Omega)^N \times L^2(\partial\Omega)$. In this case, the problem (M) can be rewritten as

$$\inf_u \mathcal{F}(u) + \mathcal{G}(K(u))$$

where $K = (\nabla, \gamma_0)$, and γ_0 is the trace operator on the boundary. This being said, at the second step of the Algorithm 1 we need to compute γ_0^* which turns requiring to solve a PDE. Indeed, we define

$$\gamma_0 : H^1(\Omega) \to L^2(\partial\Omega)$$

through $\gamma_0(u) = u_{|\partial\Omega}$ for every $u \in H^1(\Omega)$. By definition, for any $(u, v) \in H^1(\Omega) \times L^2(\partial\Omega)$

$$\langle\gamma_0 u, v\rangle_{L^2(\partial\Omega)} = \langle u, \gamma_0^* v\rangle_{H^1(\Omega)}.$$

This means that

$$\int_{\partial\Omega} uv\mathrm{d}S = \int_\Omega u(\gamma_0^* v)\mathrm{d}\mathbf{x} + \int_\Omega \nabla u\nabla(\gamma_0^* v)\mathrm{d}\mathbf{x}$$

for any $u \in H^1(\Omega)$. In other words $\gamma_0^* v$ solves the following PDE

$$-\Delta z + z = 0 \text{ in } \Omega \ \text{and} \ \partial_n z = v \text{ on } \partial\Omega.$$

Thus we opt for the first formulation in order to avoid additional costs to the computations.

4.2. Optimality conditions and stopping criterion

As usual, we can check the optimality conditions (3.11) associated to $(M)_d$ and $(OF)_d$. Namely we check the following conditions:

– Divergence error: $\| - \operatorname{div}_h(\boldsymbol{\phi}) - 1\|_2$,
– Dual error: $\|\sigma(x, \boldsymbol{\phi}) - \nabla_h u \cdot \boldsymbol{\phi}\|_1$,
– Lip error: $\sup_{i,j} \sigma^*(ih, jh, \nabla_h u_{i,j})$,

for a large number of iterations ($\sim$5000 iterations). Note that for vertical light direction, the support function σ is easy to compute. More particularly, one has for every $\mathbf{p} \in \mathbb{R}^N$, $\sigma(\mathbf{x}, \mathbf{p}) = k(\mathbf{x})|\mathbf{p}|$ where $|\mathbf{p}|$ is the Euclidean norm of $\mathbf{p}$. Thus, for the Lip error, we can check the value $\sup_{i,j}(\|\nabla_h u_{i,j}\| - k_{i,j})$. We expect that Divergence error, Dual error and Lip error to be close to zero. Then, we apply the algorithm until the difference between the functional values of u^k and $\boldsymbol{\phi}^k$ is below a certain threshold $\epsilon = 5 \times 10^{-3}$ (see Tab. 1).

4.3. Numerical examples

We test for some commonly used images: Mozart and vase images taken from [44] and Basilica and vaso images taken from [24, 25]. In these cases, the shapes are reconstructed by solving the Eikonal equation $|\nabla u(\mathbf{x})| = k(\mathbf{x})$ in 2D with $g \equiv 0$, *i.e.* with homogeneous Dirichlet boundary condition $u = 0$ on $\partial\Omega$. More precisely, we load a surface $u(\mathbf{x})$ as $2D$-field using a depth map and we compute the normal vector to the surface $(\mathbf{x}, u(\mathbf{x}))$ to get

$$I(\mathbf{x}) = \mathbf{n}(\mathbf{x}) \cdot \boldsymbol{\ell}, \ \text{with} \ \boldsymbol{\ell} = (0, 0, 1).$$

That is

$$I(\mathbf{x}) = \frac{1}{\sqrt{\|\nabla_h u(\mathbf{x})\|^2 + 1}}.$$

The algorithm was implemented in Matlab and executed on a 2, 3 GHz CPU running macOs Big Sur system. The code was executed for 5000 iterations with $\tau = 0.001$ and $\eta = 8/\tau$ for all the shapes.

Following the survey [17] the reconstructed shape for the vase (Fig. 3) is similar to the one obtained using the minimization method proposed in [16]. As for the vaso shape (Fig. 5), the obtained shape is similar to the one obtained using linear approximation of the reflectance function as in [37]. The error estimators we obtain (see Tab. 2) are better.

The estimated shape for Mozart (Fig. 7) is better than the results presented in [44] and details (nose, mouth, eyes) are clear. The estimated shape of the Basilica (Fig. 9) is a bit different from the one obtained using a semi-Lagrangian scheme in [25], where in particular, additional information is supposed on the discontinuities of the images to obtain a well-reconstructed shape. Let us stress that for all the figures only a Dirichlet boundary condition $u \equiv 0$ is imposed, which explains the flat roofs in our reconstructed Basilica compared to the one in [25].

Before ending this section, let us give several error estimators to compare the true solution with the computed one following [17]. For every known f and computable $\tilde{f}$, we define respectively the mean absolute deviation, the root mean square and the maximal absolute deviation erros

$$|\Delta f|_1 = \frac{1}{\mathcal{N}} \sum_{i=1}^{m} \sum_{j=1}^{n} \left| f_{i,j} - \tilde{f}_{i,j} \right|, \quad |\Delta f|_2 = \left[\frac{1}{\mathcal{N}} \sum_{i=1}^{m} \sum_{j=1}^{n} \left| f_{i,j} - \tilde{f}_{i,j} \right|^2 \right]^{1/2}, \quad |\Delta f|_\infty = \max_{i,j} \left| f_{i,j} - \tilde{f}_{i,j} \right| \quad (4.9)$$

where $\mathcal{N}$ is the number of grid points.

For the two vases shapes (Figs. 3–5), the error measures in Table 2 above are better than the ones presented in [17]. As for the optimality conditions (see Figs. 4–6–8–10), we see that the values are getting close to zero throughout the iterations. Yet, their order of magnitude is bigger than for the tests performed in [19]. We believe that all the results of this section could be improved using some preconditioning techniques as in [38].
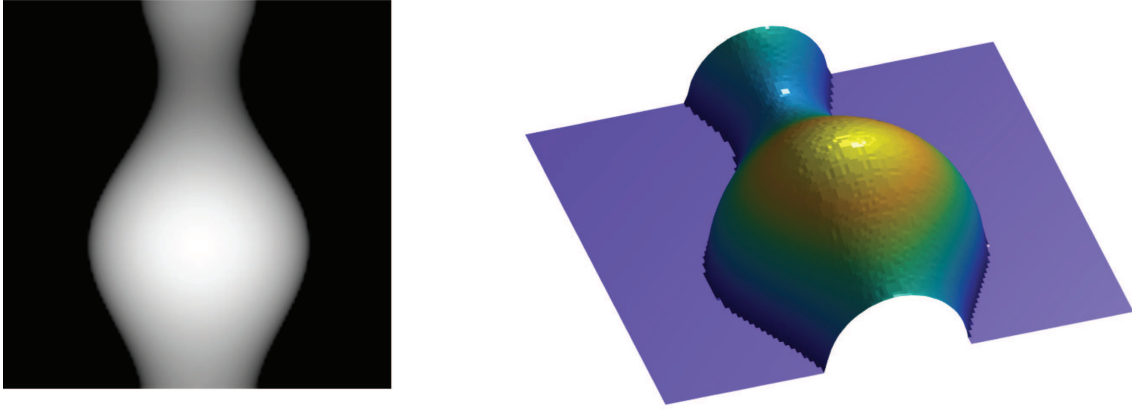
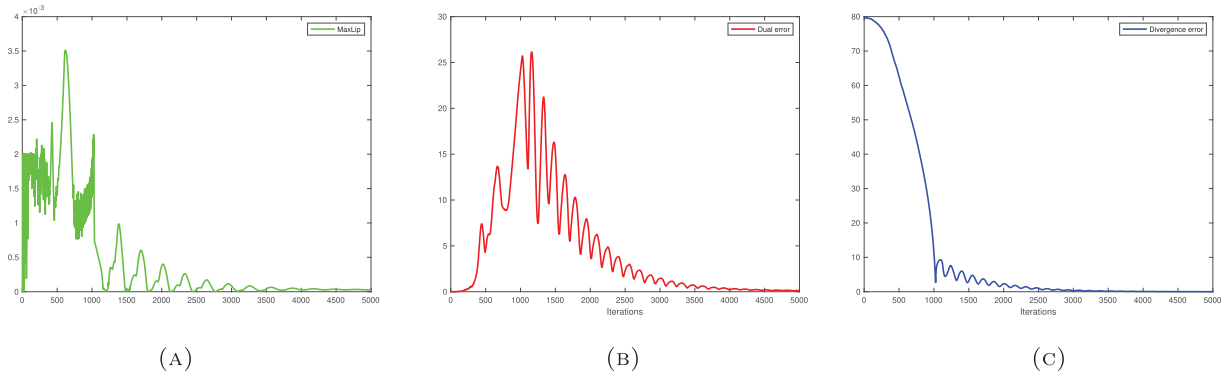FIGURE 3. *Left* to *right*: initial image, the reconstructed shape.

FIGURE 4. Optimality conditions for the vase. (A) Lip Error. (B) Dual Error. (C) Divergence Error.

FIGURE 5. *Left* to *right*: initial image, the reconstructed shape.

TABLE 1. The table presents the execution time and the number of iterations needed until the difference between the functional values of u^k and ϕ^k falls below tolerance $\epsilon = 5 \times 10^{-3}$. We observed that the choice of the parameter τ influences the error criterion as well as the allure of the reconstructed shapes, especially the Basilica and Mozart. The most time consuming step of the algorithm is indeed the computation of $\mathbf{Prox}_{\eta \mathcal{G}_h^*}$, and more precisely the projections onto $B(0, k_{i,j})$ since the other steps consist in simple vectorial operations.

Shape	Execution time in seconds	Number of iterations
vase	2.98 s	1019
vaso	8.45 s	1047
Mozart	7.86 s	1051
Basilica	6.82 s	834

TABLE 2. Error measures on the different shapes.

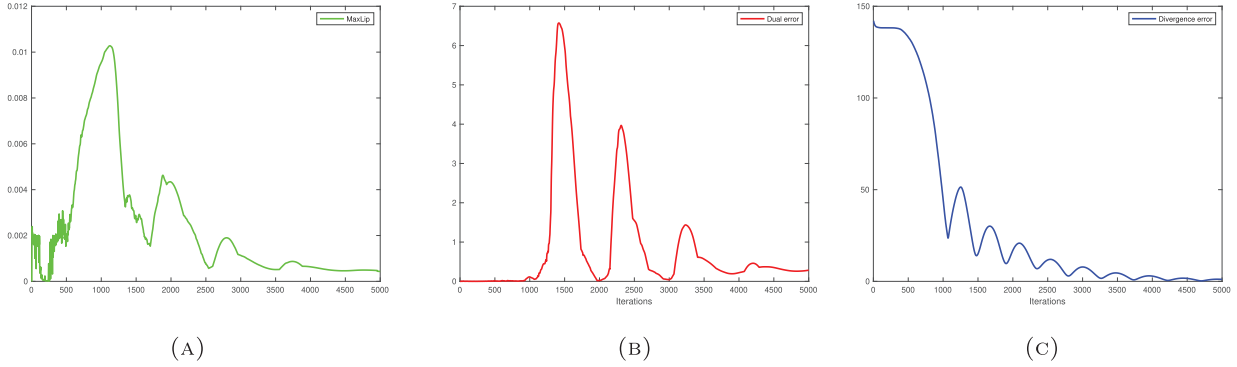|	$|\Delta u|_1$	$|\Delta u|_2$	$|\Delta u|_\infty$	$|\Delta \mathbf{n}|_1$	$|\Delta \mathbf{n}|_2$	$|\Delta \mathbf{n}|_\infty$	$|\Delta I|_1$	$|\Delta I|_2$	$|\Delta I|_\infty$
vase	1.54e-03	3.56e-03	2.24e-02	3.46e-06	8.05e-06	8.26e-05	1.39e-04	2.77e-04	2.48e-03
vaso	1.61e-02	3.75e-02	2.47e-01	1.36e-05	1.84e-04	1.54e-02	1.32e-03	5.61e-03	2.02e-01
Mozart	1.96e-02	3.65e-02	1.46e-01	9.06e-06	1.21e-04	1.08e-02	1.26e-03	2.73e-03	7.68e-02
Basilica	1.13e-02	2.51e-02	1.66e-01	5.46e-05	1.05e-03	6.32e-02	7.47e-04	4.17e-03	1.46e-01

(A) (B) (C)

FIGURE 6. Optimality conditions for the vaso. (A) Lip Error. (B) Dual Error. (C) Divergence Error.

Remark 4.2. Define the so called primal-dual gap

$$\mathrm{G}(u, \phi) := \mathcal{F}_h(u) + \mathcal{G}_h(\nabla_h u) + \mathcal{F}_h^*(\mathrm{div}(\phi)) + \mathcal{G}_h^*(\phi). \tag{4.10}$$

Since $\mathrm{G}(u, \phi)$ vanishes if and only if (u, ϕ) is a saddle point, one can use the primal-dual gap to terminate the iteration and check the optimality conditions by verifying that $\mathrm{G}(u, \phi) < \epsilon$ for a given tolerance ϵ. However, this turns to be not useful in practice due to the presence of the indicator functions $\mathcal{G}_h$ and $\mathcal{F}_h^*$.

Remark 4.3. The approach presented in this paper for the SfS problem is intimately related to some optimal transport problems. Indeed, the duality result given by Theorem 2.3 says that the solution u is in some sense the Kantorovich potential for the mass transport problem between the Lebesgue measure $\alpha = \mathcal{L}^N \llcorner \Omega$ (the restriction of Lebesgue measure to the domain Ω) and an unknown measure β concentrated on $\partial\Omega$ which is
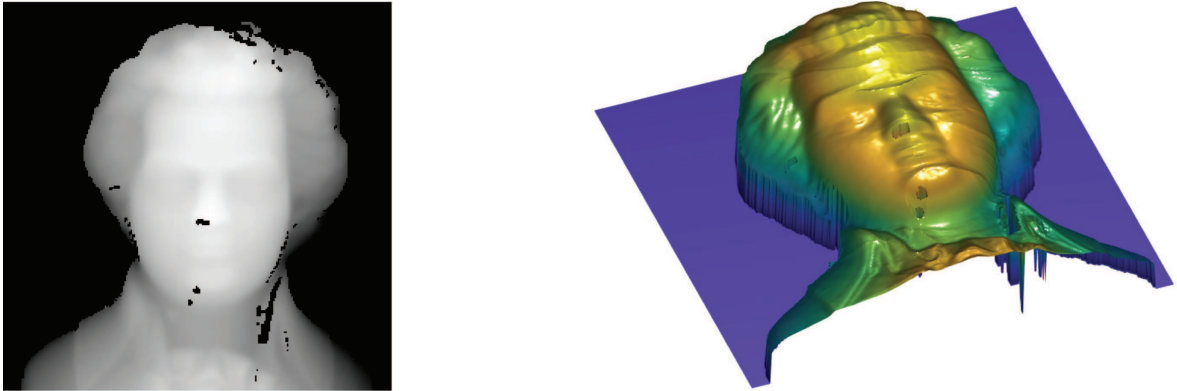
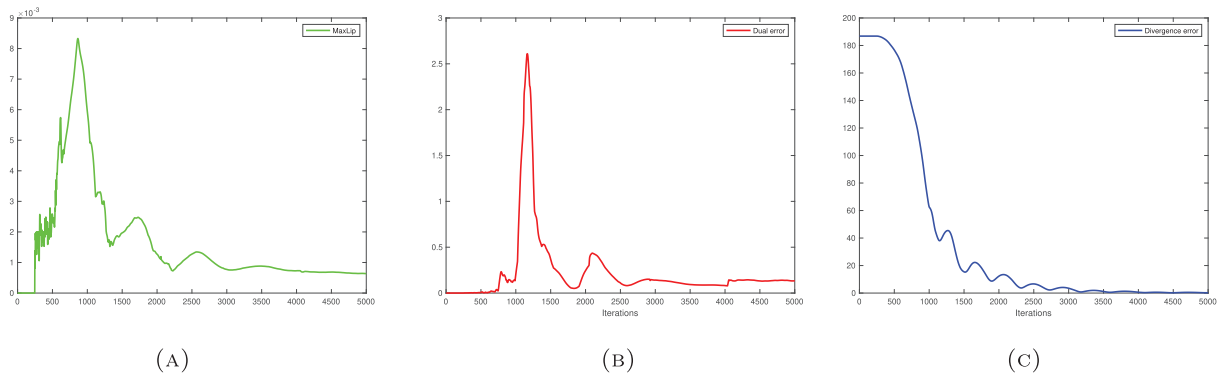FIGURE 7. *Left* to *right*: initial image, the reconstructed shape.

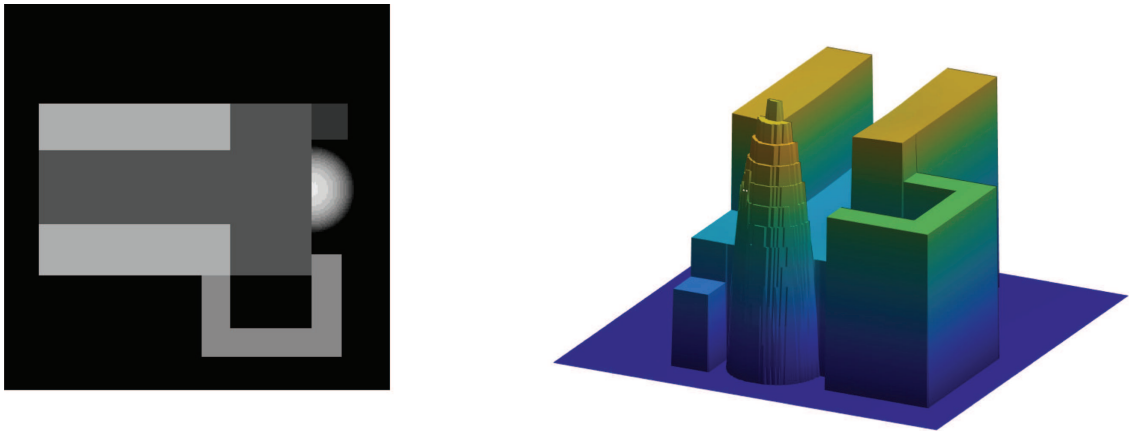FIGURE 8. Optimality conditions for Mozart. (A) Lip Error. (B) Dual Error. (C) Divergence Error.

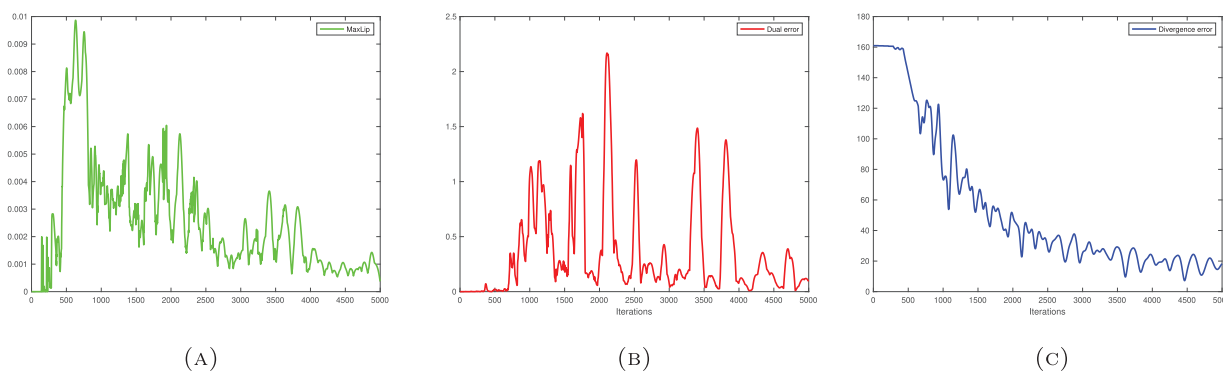FIGURE 9. *Left* to *right*: initial image, the reconstructed shape.

FIGURE 10. Optimality conditions for the Basilica. (A) Lip Error. (B) Dual Error. (C) Divergence Error.
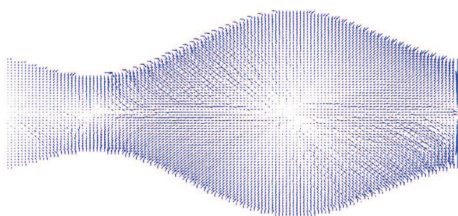

FIGURE 11. The optimal flow ϕ for the vase.

related to the trace of the optimal flow ϕ (see [20] for details). Recall that the flow field ϕ (see Fig. 11) describes how the mass moves locally. In Figure 12 we see the evolution of the shape of the vase through iterations. This is somehow related to the evolution of the initial shape of a sandpile by considering (at least formally) the limit as $t \to \infty$ in the differential inclusion

$$\alpha \in \partial_t u + \partial \mathbb{I}_{B_{\sigma^*}}(u), \tag{4.11}$$

with $\alpha = \mathcal{L}^N \llcorner \Omega$ and $\partial \mathbb{I}_{B_{\sigma^*}}$ is the L^2-subdifferential of B_{σ^*}. The inclusion (4.11) can be discretized using a minimizing movement scheme la Jordan-Kinderlehrer-Otto [32] with the 1-Wassertstein distance induced by the metric d_σ in the spirit of [1]. These connections are worth being investigated in depth and may give rise to many applications.

5. CONCLUSIONS, COMMENTS AND EXTENSIONS

In the present paper we proposed a primal-dual algorithm for a class of SfS problem taking advantage of the variational formulation for HJ equations (*cf.* [19]). The approach adds to the different families of methods and techniques developed to tackle this problem (see [4, 15, 21, 26, 29, 34, 36, 37, 39, 41]) and can be positioned between the PDE and optimization methods treating the SfS problem. We believe that recovering the solution of HJ equations *via* a maximization problem has several advantages amongst them by the fact that one can take advantage of the recent advances in optimization methods, namely in primal-dual algorithms to get improved results. In addition, this allows handling the so-called concave/convex ambiguity. Moreover, the strategy works (at least theoretically) to oblique light direction as one needs to solve a PDE of the form

$$\begin{cases} H(\mathbf{x}, \nabla u) = 0 & \text{in } \Omega \\ u = 0 & \text{on } \partial\Omega. \end{cases} \tag{5.1}$$
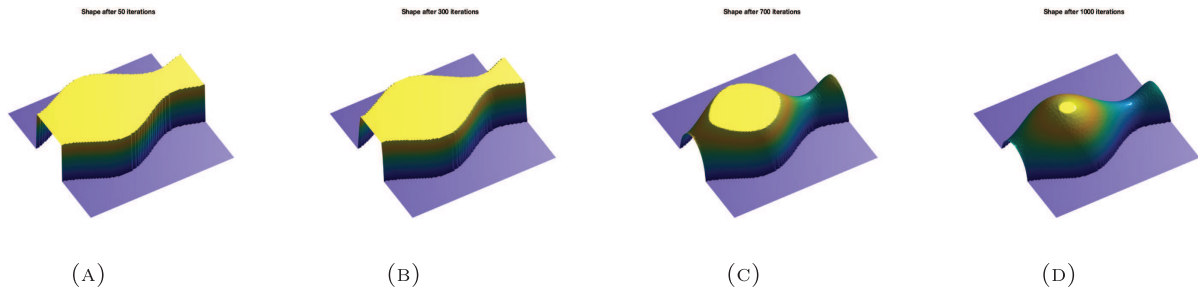
FIGURE 12. Evolution of the vase shape during iterations. (A) 50 iterations. (B) 300 iterations. (C) 700 iterations. (D) 1000 iterations.

Similarly, the maximal viscosity subsolution of (5.1) can be recovered *via* the following maximization problem

$$(M): \quad \max_{u \in W^{1,\infty}(\Omega)} \left\{ \int_\Omega u \mathrm{d}\mathbf{x} : \quad \sigma^*(\mathbf{x}, \nabla u) \leq 1, \quad u = 0 \text{ on } \partial\Omega \right\}. \tag{5.2}$$

Note that in this case, the convergence of the discretization (see Prop. 3.2) remains true. The main difficulty lies in the fact that computing $\mathbf{Prox}_{\mathcal{G}^*}$ in Algorithm 1 will require performing projections onto

$$Z(\mathbf{x}) = \{\mathbf{p} \in \mathbb{R}^N : \ H(\mathbf{x}, \mathbf{p}) \leq 0\},$$

for every $\mathbf{x} \in \Omega$ (see [19], Prop. 2.5) instead of Euclidean balls as it was the case of vertical light source. This can be tedious for general convex set $Z(\mathbf{x})$. Let us stress that Neumann boundary conditions can also be considered. Indeed, by analogy with the formulation in Remark 4.1, the same consideration suggest considering the problem (M) by taking $K = (\nabla, \partial_\nu)$ with ∂_ν being the normal derivative. This being said, Algorithm 1 will require computing the adjoint operator K^*. We are planning to address these questions in future works.

REFERENCES

[1] M. Agueh, G. Carlier and N. Igbida, On the minimizing movement with the 1-Wasserstein distance. *ESAIM Control Optim. Calc. Var.* **24** (2018) 1415–1427.

[2] A. Ahmed and A. Farag, A new formulation for shape from shading for non-Lambertian surfaces. In: IEEE Computer Society Conference on Computer Vision and Pattern Recognition. Vol. 2 (2006) 1817–1824.

[3] L. Ambrosio, N. Fusco and D. Pallara, Functions of Bounded Variation and Free Discontinuity Problems. Clarendon Press, Oxford (2000).

[4] M. Bardi and M. Falcone, Discrete approximation of the minimal time function for systems with regular optimal trajectories. In: Analysis and Optimization of Systems. *Lect. Notes Control Inf. Sci.* Vol. 144 (1990) 103–112.

[5] J.-D. Benamou and G. Carlier, Augmented Lagrangian methods for transport optimization, mean field games and degenerate elliptic equations. *J. Optim. Theory Appl.* **167** (2015) 1–26.

[6] F. Boyer and P. Fabrie, Mathematical Tools for the Study of the Incompressible Navier–Stokes Equations and Related Models. Vol. 183 of *Applied Mathematical Sciences*. Springer, New York (2013).

[7] F. Camilli and L. Grüne, Numerical approximation of the maximal solutions for a class of degenerate Hamilton–Jacobi equations. *SIAM J. Numer. Anal.* **38** (2000) 1540–1560.

[8] F. Camilli and A. Siconolfi, Maximal subsolutions for a class of degenerate Hamilton–Jacobi problems. *Indiana Univ. Math. J.* **48** (1999) 1111–1131.

[9] F. Camilli and S. Tozza, A unified approach to the well-posedness of some non-Lambertian models in shape-from-shading theory. *SIAM J. Imaging Sci.* **10** (2017) 26–46.

[10] A. Chambolle, An algorithm for total variation minimization and applications. *J. Math. Imaging Vis.* **20** (2004) 89–97.

[11] A. Chambolle and T. Pock, A first-order primal-dual algorithm for convex problems with applications to imaging. *J. Math. Imaging Vis.* **40** (2011) 120–145.

[12] F. Courteille, A. Crouzil, J.-D. Durou and P. Gurdjos, Towards shape from shading under realistic photographic conditions. In: Proceedings of the 17th International Conference on Pattern Recognition. Vol. 2 (2004) 277–280.

[13] M.G. Crandall and P.-L. Lions, Viscosity solutions of Hamilton–Jacobi equations. *Trans. Am. Math. Soc.* **277** (1983) 1–42.

[14] M.G. Crandall, H. Ishii and P.-L. Lions, User's guide to viscosity solutions of second order partial differential equations. *Bull. Am. Math. Soc. New Ser.* **27** (1992) 1–67.

[15] A. Crouzil, X. Descombes and J.-D. Durou, A multiresolution approach for shape from shading coupling deterministic and stochastic optimization. *IEEE Trans. Pattern Anal. Mach. Intell.* **25** (2003) 1416–1421.

[16] P. Daniel and J.-D. Durou, From deterministic to stochastic methods for shape from shading. In: Proc. 4th Asian Conf. Comp. Vis. (2000).

[17] J.-D. Durou, M. Falcone and M. Sagona, Numerical methods for shape-from-shading: a new survey with benchmarks. *Comput. Vis. Image. Underst.* **109** (2008) 22–43.

[18] S. Dweik and F. Santambrogio, Summability estimates on transport densities with Dirichlet regions on the boundary via symmetrization techniques. *ESAIM Control Optim. Calc. Var.* **24** (2018) 1167–1180.

[19] H. Ennaji, N. Igbida and V.T. Nguyen, Augmented Lagrangian methods for degenerate Hamilton–Jacobi equations. *Calc. Var. Part. Differ. Equ.* **60** (2021) 238.

[20] H. Ennaji, N. Igbida and V.T. Nguyen, Beckmann-type problem for degenerate Hamilton–Jacobi equations. *Quart. Appl. Math.* (2021) (in press) DOI: 10.1090/qam/1606.

[21] M. Falcone, T. Giorgi and P. Loreti, Level sets of viscosity solutions: some applications to fronts and Rendez-Vous problems. *SIAM J. Appl. Math.* **54** (1994) 1335–1354.

[22] M. Falcone, M. Sagona and A. Seghini, A scheme for the shape-from-shading model with black shadows. In: Numerical Mathematics and Advanced Applications (2003) 503–512.

[23] A. Fathi and A. Siconolfi, PDE aspects of Aubry-Mather theory for quasiconvex Hamiltonians. *Calc. Var. Partial Differ. Equ.* **22** (2005) 185–228.

[24] A. Festa, *Analysis and approximation of Hamilton Jacobi equations on irregular data.* Ph.D. thesis, University of Rome, Sapienza (2012).

[25] A. Festa and M. Falcone, An approximation scheme for an Eikonal equation with discontinuous coefficient. *SIAM J. Numer. Anal.* **52** (2014) 236–257.

[26] H. Hayakawa, S. Nishida, Y. Wada and M. Kawato, A computational model for shape estimation by integration of shading and edge information. *Neural Netw.* **7** (1994) 1193–1209.

[27] B.K. Horn, Shape from shading: a method for obtaining the shape of a smooth opaque object from one view. Technical report, USA (1970).

[28] B.K.P. Horn, Obtaining Shape from Shading Information. MIT Press, Cambridge, USA (1989) 123–171.

[29] B.K.P. Horn and M.J. Brooks, The variational approach to shape from shading. *Comput. Vis. Graph. Image Process.* **33** (1986) 174–208.

[30] N. Igbida and V.T. Nguyen, Augmented Lagrangian method for optimal partial transportation. *IMA J. Numer. Anal.* **38** (2018) 156–183.

[31] N. Igbida, V.T. Nguyen and J. Toledo, On the uniqueness and numerical approximations for a matching problem. *SIAM J. Optim.* **27** (2017) 2459–2480.

[32] R. Jordan, D. Kinderlehrer and F. Otto, The variational formulation of the Fokker-Planck equation. *SIAM J. Math. Anal.* **29** (1998) 1–17.

[33] P.-L. Lions, Generalized solutions of Hamilton–Jacobi equations. In: Research Notes in Mathematics. Vol. 69. Pitman Advanced Publishing Program, Boston – London – Melbourne (1982).

[34] P.L. Lions, E. Rouy and A. Tourin, Shape-from-shading, viscosity solutions and edges. *Numer. Math.* **64** (1993) 323–353.

[35] R. Monneau, Introduction to the fast marching method (2010). https://hal.archives-ouvertes.fr/hal-00530910

[36] A.P. Pentland, Local shading analysis. *IEEE Trans. Pattern Anal. Mach. Intell.* **PAMI-6** (1984) 170–187.

[37] T. Ping-Sing and M. Shah, Shape from shading using linear approximation. *Image Vis. Comput.* **12** (1994) 487–498.

[38] T. Pock and A. Chambolle, Diagonal preconditioning for first order primal-dual algorithms in convex optimization. In: 2011 International Conference on Computer Vision (2011) 1762–1769.

[39] E. Prados, F. Camilli and O. Faugeras, A viscosity solution method for shape-from-shading without image boundary data. *ESAIM: M2AN* **40** (2006) 393–412.

[40] Y. Quéau, J. Mélou, F. Castan, D. Cremers and J.-D. Durou, A variational approach to shape-from-shading under natural illumination. In: International Conference on Energy Minimization Methods in Computer Vision and Pattern Recognition (2018) 342–357.

[41] E. Rouy and A. Tourin, A viscosity solutions approach to shape-from-shading. *SIAM J. Numer. Anal.* **29** (1992) 867–884.

[42] A. Tankus, N. Sochen and Y. Yeshurun, Shape-from-shading under perspective projection. *Int. J. Comput. Vision* **63** (2005) 21–43.

[43] S. Tozza and M. Falcone, Analysis and approximation of some shape-from-shading models for non-Lambertian surfaces. *J. Math. Imaging Vision* **55** (2016) 153–178.

[44] R. Zhang, P.-S. Tsai, J.E. Cryer and M. Shah, Shape from shading: a survey. *IEEE Trans. Pattern Anal. Mach. Intell.* **21** (1999) 690–706.

Subscribe to Open (S2O)
A fair and sustainable open access model

This journal is currently published in open access under a Subscribe-to-Open model (S2O). S2O is a transformative model that aims to move subscription journals to open access. Open access is the free, immediate, online availability of research articles combined with the rights to use these articles fully in the digital environment. We are thankful to our subscribers and sponsors for making it possible to publish this journal in open access, free of charge for authors.

Please help to maintain this journal in open access!

Check that your library subscribes to the journal, or make a personal donation to the S2O programme, by contacting subscribers@edpsciences.org

More information, including a list of sponsors and a financial transparency report, available at: https://www.edpsciences.org/en/maths-s2o-programme